

The NLO QCD corrections to $B_c(B_c^*)$ production around the Z pole at an e^+e^- collider

Xu-Chang Zheng^{a,c*}, Chao-Hsi Chang^{a,b,c†}, Tai-Fu Feng^{a,d‡}, Zan Pan^{a,c§}

^a *Key Laboratory of Theoretical Physics, Institute of Theoretical Physics, Chinese Academy of Sciences, Beijing 100190, China*

^b *CCAST (World Laboratory), P.O.Box 8730, Beijing 100190 China*

^c *School of Physical Sciences, University of Chinese Academy of Sciences, Beijing 100049, China and*

^d *Department of Physics, Hebei University, Baoding, 071002, China*

The production of B_c and B_c^* mesons at Z -factory (an e^+e^- collider running at energies around the Z pole) is calculated up-to the next-to-leading order (NLO) QCD corrections. The results show that the dependence of the total cross sections on the renormalization scale μ is suppressed by the corrections, and the NLO corrections enhance the total cross sections for B_c by 52% and for B_c^* by 33%, when the renormalization scale is taken at $\mu = 2m_b$. To observe the various behaviors of the production of the mesons B_c and B_c^* , such as the differential cross section vs. the out-going angle, the forward-backward asymmetry and the distribution vs. the energy fraction z up-to QCD NLO accuracy as well as the relevant K -factor (NLO to LO) for the production are computed and it is pointed out that some of the observables obtained here may be used as specific precision test of the Standard Model.

Keywords: B_c meson, production, Z -factory

PACS numbers: 13.66.Bc, 13.87.Fh, 14.70.Hp, 14.40.-n, 14.20.-c,

I. INTRODUCTION

The meson B_c (and its anti-particle \bar{B}_c), being an explicitly heavy-flavored quark-antiquark ground bound-state, is unique in the Standard Model (SM). The two components inside it move non-relativistically due to heavy masses of its components, so the potential model can describe the spectrum of the binding system quite reliably[1], and the nonrelativistic quantum chromodynamics effective theory (NRQCD)[2] may be adopted to compute its production, and with the effective theory for the weak interaction which is based on SM its decays may be computed[3–5], thus it specially interests us, particularly, since it was observed by CDF collaboration firstly[6].

Since the observations on the meson B_c (and its anti-particle \bar{B}_c) are available only at high energy hadronic colliders so far, so the theoretical and experimental studies of the B_c production mostly focus on its hadronic production[4, 5]. According to QCD factorization theorem the hadronic production of a hadron, e.g. B_c meson, always is through the collision of the partons inside the colliding hadrons stochastically, while the momentum fraction of the colliding hadron, carried by the colliding partons, is determined by the parton distribution function (PDF) of the colliding hadron, so the total colliding energy and the moving in longitudinal direction of the center-of-mass system (C.M.S.) of the colliding partons cannot be controlled, thus only the perpendicular

components of the momenta of the products, which are measurable, have proper meaning in understanding the production. Namely to observe the production through hadron collision can acquire quite restrictive knowledge about the production.

In contrary, for the production of the meson B_c (and its anti-particle \bar{B}_c) via e^+e^- collisions, the C.M.S. of the 'subprocess' precisely is of $e^+ + e^-$ collisions, so the observables, such as all components of the momenta of the products, the angle distributions and the 'forward-backward asymmetry' of the concerned product to the direction of the colliding e^+ or e^- etc, have proper meaning in studying the production, even may be used to test of the Standard Model, thus to study B_c meson production at an e^+e^- collider is very important and interesting. Especially the collisions happen to take place at a Z -factory (e^+e^- colliders running at energies around the Z pole), the production will be enhanced greatly by the resonance effect. Now several suggestions on Z -factories, e^+e^- facilities run at energies around the Z pole with much higher luminosity than that of LEP-I, e.g. ILC, CEPC and FCC-ee, are proposed, thus at a modernized Z -factory with very very high luminosity the production must achieve a lot of new knowledge, although the B_c meson production at LEP-I (an old Z -factory) is too small to be observed[7, 8]. Indeed concerning the possible Z -factory being under consideration, in Ref.[9] the production of doubly heavy flavored hadrons (B_c meson and baryons $\Xi_{cc}, \Xi_{bc}, \Xi_{bb}$ etc and their excited states as well as their antiparticle) via e^+e^- collision at the energy around the Z pole is re-studied but only under the approach of complete QCD at the leading order (LO) and the fragmentation approach at the leading logarithm order (LL) thoroughly. In Ref.[9] it is found that the LO results have quite remarkable dependence

*e-mail:zhengxc@itp.ac.cn

†e-mail:zhangzx@itp.ac.cn

‡email:fengt@hbu.edu.cn

§e-mail:panzan@itp.ac.cn

on the renormalization scale, although certain interesting results, such as the precise asymmetries in forward-backward and lefthand-righthand in $B_c(B_c^*)$ production, are obtained. In order to have more precise theoretical prediction and to suppress the dependence on the renormalization scale, it certainly is requested to carry out the computations on the $B_c, (B_c^*)$ meson production at a Z -factory up-to the QCD NLO accuracy. Thus we devote ourselves to doing it here.

Since B_c and its excited states such as $B_c^*, B_c^{**} \dots$ carry two heavy-flavors explicitly, so the excited states $B_c^*, B_c^{**} \dots$ will decay (or cascade-decay) to the ground state, B_c , through strong or electromagnetic interaction with almost 100% probability, thus as Ref.[9], here the production of the excited state $B_c^* (^3S_1, J^P = 1^-)$, the lowest excited state of B_c , is also computed up-to QCD NLO.

According to NRQCD[2], the production of $B_c(B_c^*)$ meson by electron-positron collision can be factorized into two factors at a specific energy μ_F in QCD perturbative region: one is the electron-positron production of the 'free' c, \bar{b} quark pair inclusively in short distance, which can be calculated by perturbative QCD (pQCD), and the other one is to depict how the produced c and \bar{b} quarks to form the meson $B_c(B_c^*)$, which is nonperturbative but can be achieved phenomenologically or via potential model (the wave function at origin) etc. Here setting the factorization energy scale μ_F is equal to the renormalization one μ_R , for the former factor we compute the production up-to next leading order (NLO) QCD corrections, and for the later factor we consider the leading order in relative velocity v between the two heavy quarks inside the meson $B_c(B_c^*)$ only. For convenience, later on we denote $\mu \equiv \mu_F = \mu_R$ throughout the paper.

The paper is organised as follows: Following the Introduction, in Section II, we briefly recall the useful formulas to the LO accuracy. In Section III, we present the approaches to compute the NLO corrections of QCD for the B_c (and B_c^*) meson production at a Z -factory. In Section IV, with the necessary parameters being given, the numerical results are presented. Section V is devoted to discussions and summary. In Appendix-A, it is shown how the relevant width of the production of B_c meson and B_c^* meson by Z decay are derived from the total cross sections of the production at a Z -factory and in Appendix-B precise comparisons between the relevant widths derived from the total cross sections of the production at a Z -factory computed here and directly computed from the Z decay, which appear in literature.

II. THE CROSS SECTION UP-TO LEADING ORDER (LO)

There are four Feynman diagrams for the B_c and B_c^* production at LO accuracy, only two of them are presented in Fig.1, but the other two can be obtained by interchanging the b -quark and c -quark lines in Fig.1.

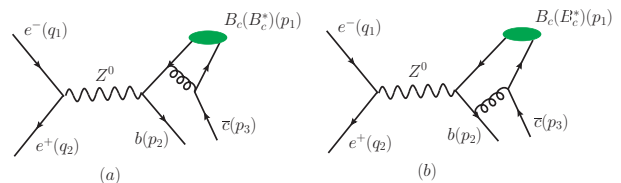


FIG. 1: Two of the four Feynman diagrams to LO accuracy for the production $e^-(q_1) + e^+(q_2) \rightarrow B_c(B_c^*)(p_1) + b(p_2) + \bar{c}(p_3)$.

Note that in the present paper the studies focus on the production from QCD LO accuracy up-to QCD NLO accuracy, but merely when the $e^+ + e^-$ collider runs around the Z pole. Thus the contributions corresponding to the Feynman diagrams with Z -boson mediation are dominant and we will compute them carefully, but those corresponding to the Feynman diagrams with γ mediation are approximately ignored¹. Under the approximation the computations for QCD LO and QCD NLO are simplified quite a lot, and at the end of Section IV we also estimate how well the approximation is by taking into account the contributions from the Feynman diagrams with γ mediation, i.e. those from the γ mediation itself being squared and those corresponding to the interference of the γ mediation and Z -boson mediation.

The cross section to QCD LO can be formulated as:

$$d\sigma_{\text{LO}} = \frac{1}{4} \frac{1}{2s} \sum |M_{\text{LO}}|^2 d\Phi_3, \quad (1)$$

where $\frac{1}{2s}$ is the flux factor; \sum means that the spins and the colors in the initial and final states are summed over; $1/4$ comes from the spin average of the initial e^+e^- ; $d\Phi_3$ denotes the three-body phase space for the final states and M_{LO} is the LO Feynman amplitude, which is the sum of four terms for the LO Feynman diagrams. The details about M_{LO} can be found in Ref.[9].

III. THE NLO QCD CORRECTIONS

The NLO QCD corrections for the process $e^+ + e^- \rightarrow B_c(B_c^*) + b + \bar{c}$ include virtual and real ones. The half of the Feynman diagrams for the virtual correction are those in Figs.2,3,4,5, and the half of the Feynman diagrams for the real correction are those in Fig.6. The other half of the Feynman diagrams for the virtual corrections and for real corrections can be also obtained by interchanging the b -quark and c -quark lines in Figs.2~6.

To the QCD NLO accuracy, the cross section is formulated as

$$\sigma_{\text{NLO}} = \sigma_{\text{LO}} + \sigma_{\text{Virtual}} + \sigma_{\text{Real}}. \quad (2)$$

¹ Thus without special statement, in the Feynman diagrams Figs.1,2,3,4,5,6 the Z mediation diagrams are involved only, but the ones with the γ mediation are not.

Here σ_{Virtual} denotes the so-called virtual correction and σ_{Real} denotes the so-called real correction. Now let us

calculate them respectively.

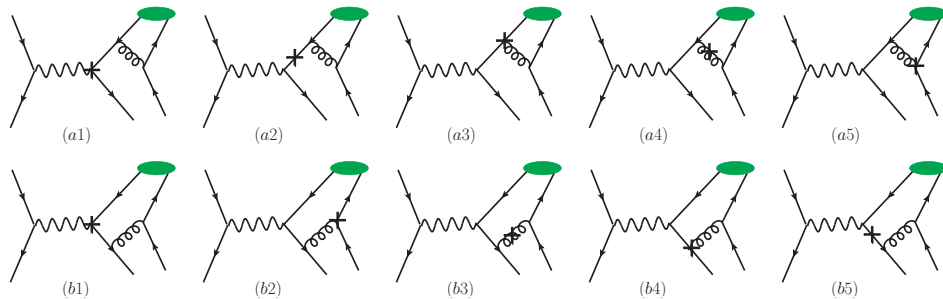


FIG. 2: The half of Feynman diagrams containing a ‘counterterm’ (denoted by \times) in need of consideration for the NLO QCD production $e^- + e^+ \rightarrow B_c(B_c^*) + b + \bar{c}$.

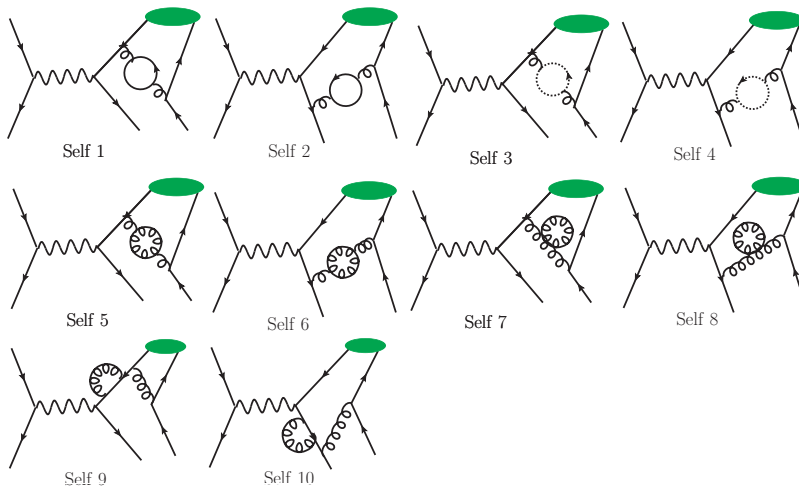


FIG. 3: The half of Feynman diagrams containing a ‘self-energy’ part for the virtual correction in need of computation for the NLO QCD production $e^-(q_1) + e^+(q_2) \rightarrow B_c(B_c^*)(p_1) + b(p_2) + \bar{c}(p_3)$.

A. The NLO QCD virtual correction

The virtual correction up-to QCD NLO is to consider the interference of the LO ones and those corresponding to the correction Feynman diagrams, i.e. Figs.2,3,4,5 and those with the c -quark and b -quark lines being interchanged. Thus the virtual correction to the cross section can be formulated as

$$d\sigma_{\text{Virtual}} = \frac{1}{4} \frac{1}{2s} \sum 2\text{Re}(M_{\text{LO}}^* M_{\text{Virtual}}) d\Phi_3. \quad (3)$$

There are ultraviolet (UV) and infrared (IR) divergences in the amplitudes corresponding to the correction Feynman diagrams. We adopt dimensional regularization with $D = 4 - 2\epsilon$ to isolate the UV and IR divergences. There are the Coulomb divergences in the conventional

matching procedure, which should be absorbed into the binding potential for the two heavy quarks inside the B_c and B_c^* . In the dimensional regularization, there is a simpler way to extract the NRQCD short-distance coefficients directly using the method of regions[10], i.e., expanding the amplitudes with the relative momentum (q) of the constituent quarks before performing loop integration, and in the lowest non-relativistic approximation for the S -wave states of the binding system $c\bar{b}$, only the terms with $q = 0$ are taken. Thus we don't confront the contributions from the low energy regions such as those from the potential region.

In dimensional regularization, γ_5 should be treated carefully. We adopt the reading point prescription[11]. It has the following rules,

- The anticommutation relation $\{\gamma_5, \gamma^\mu\} = 0$ is valid.

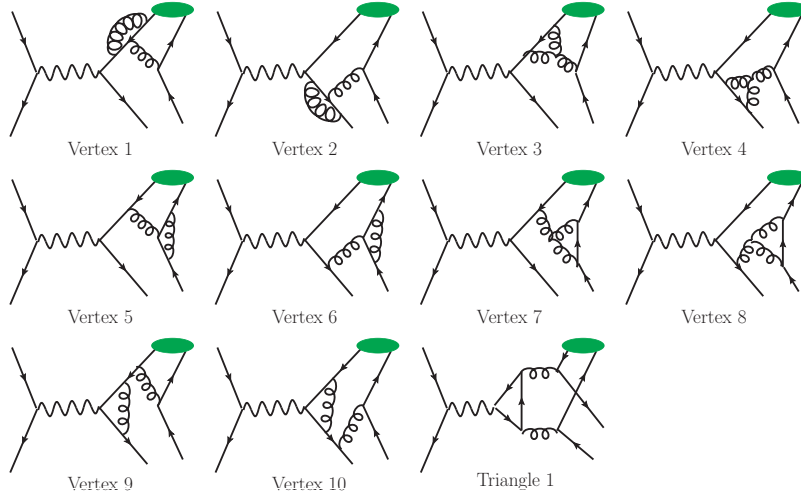


FIG. 4: The half of Feynman diagrams containing a vertex or a triangle part for the virtual correction in need of computation for the NLO QCD production $e^-(q_1) + e^+(q_2) \rightarrow B_c(B_c^*)(p_1) + b(p_2) + \bar{c}(p_3)$.

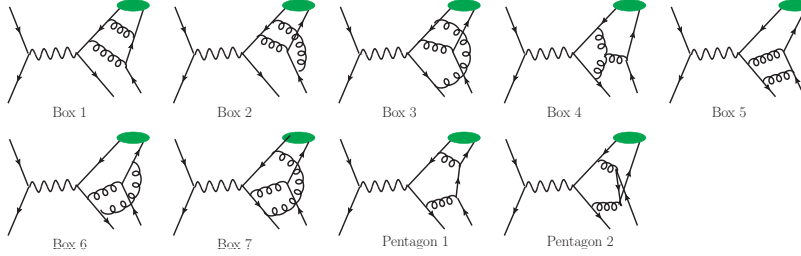


FIG. 5: The half of Feynman diagrams containing a 'box' or a 'pentagon' part for the virtual correction in need of computation for the NLO QCD production $e^-(q_1) + e^+(q_2) \rightarrow B_c(B_c^*)(p_1) + b(p_2) + \bar{c}(p_3)$.

Thus after applying the anticommutation relation and $\gamma_5^2 = 1$, there is one or no γ_5 in each Dirac trace.

- Cyclic manipulation in the Dirac traces is prevented. When considering the contributions from several diagrams, for all of them the traces in the amplitude (or resulting from squared fermionic amplitudes) must be read with starting from the same vertex respectively.
- The relevant axial current anomalies would be obtained and the conservation for vector currents is guaranteed by starting all the traces with the axial vector vertex.

Here the UV divergences come from self-energy, vertex and triangle diagrams only², which are canceled by the counterterms through renormalization, and here the

² The UV divergence from the amplitude of the anomalous diagram Triangle-1 in Fig.4 is canceled by the UV divergence from the other anomalous diagram.

renormalization scheme is that the renormalization constants Z_2 , Z_m , and Z_3 , which correspond to the renormalization of quark field, quark mass and gluon field, are determined by the renormalization of the on-mass-shell scheme (OS), whereas Z_g relating to the strong coupling constant α_s is determined by the renormalization of the modified-minimal-subtraction scheme (\overline{MS}). Then with the renormalization, we have:

$$\begin{aligned} \delta Z_2^{OS} &= -C_F \frac{\alpha_s}{4\pi} \left[\frac{1}{\epsilon_{UV}} + \frac{2}{\epsilon_{IR}} - 3\gamma_E + 3 \ln \frac{4\pi\mu^2}{m^2} + 4 \right], \\ \delta Z_m^{OS} &= -3 C_F \frac{\alpha_s}{4\pi} \left[\frac{1}{\epsilon_{UV}} - \gamma_E + \ln \frac{4\pi\mu^2}{m^2} + \frac{4}{3} \right], \\ \delta Z_3^{OS} &= \frac{\alpha_s}{4\pi} \left[(\beta'_0 - 2C_A) \left(\frac{1}{\epsilon_{UV}} - \frac{1}{\epsilon_{IR}} \right) \right. \\ &\quad \left. - \frac{4}{3} T_F \left(\frac{1}{\epsilon_{UV}} - \gamma_E + \ln \frac{4\pi\mu^2}{m_c^2} \right) \right. \\ &\quad \left. - \frac{4}{3} T_F \left(\frac{1}{\epsilon_{UV}} - \gamma_E + \ln \frac{4\pi\mu^2}{m_b^2} \right) \right], \\ \delta Z_g^{\overline{MS}} &= -\frac{\beta_0}{2} \frac{\alpha_s}{4\pi} \left[\frac{1}{\epsilon_{UV}} - \gamma_E + \ln(4\pi) \right], \end{aligned} \quad (4)$$

where m appearing in δZ_2^{OS} and δZ_m^{OS} represents the

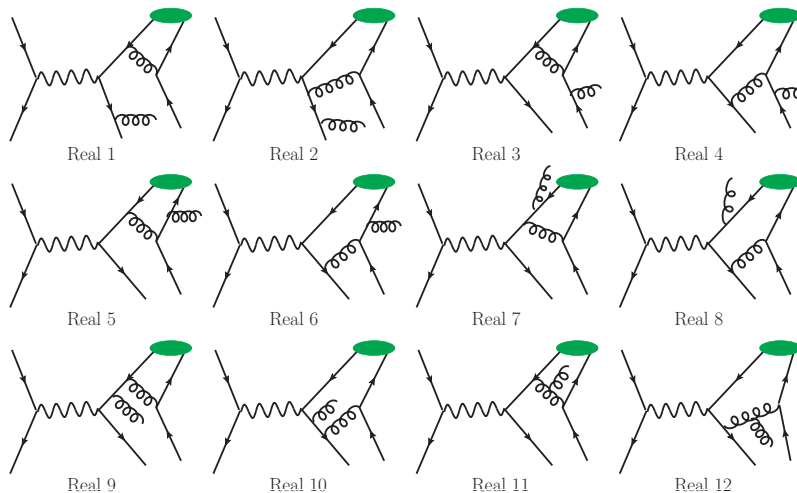


FIG. 6: The half of the Feynman diagrams for the real correction in need of computation for the NLO QCD production $e^-(q_1) + e^+(q_2) \rightarrow B_c(B_c^*)(p_1) + b(p_2) + \bar{c}(p_3)$.

mass m_b or m_c accordingly, μ is the energy where the renormalization is carried out, and γ_E is Euler's constant. $\beta_0 = \frac{11}{3}C_A - \frac{4}{3}T_F n_f$ is the one-loop coefficient of the QCD β -function, and n_f is the number of active quark flavors. Here for the concerned process, there are three light quarks u, d, s and two heavy quarks c, b , so $n_f = 5$. But in Eq.(4) precisely $\beta'_0 = \frac{11}{3}C_A - \frac{4}{3}T_F n_{lf}$, and $n_{lf} = 3$ for the light quark flavors. For $SU(3)_c$ group, $C_A = 3$, $T_F = \frac{1}{2}$ and $C_F = \frac{4}{3}$. Because there is no external gluon line at LO level, δZ_3 is canceled at NLO total amplitude level, so the final results are independent of the renormalization scheme of the gluon field.

The IR divergences in the Feynman diagrams for the virtual correction can be well analyzed[12, 13]. For the concerned process, the IR divergences come from the vertex, box and pentagon diagrams. Of Fig.4, only the amplitudes corresponding to diagrams Vertex-5 and Vertex-6 have IR divergences. Of Fig.5, except Box-4, the rests have IR divergences. The other half of the Feynman diagrams, which are obtained from Figs.4~5 by interchanging the c -quark and b -quark lines, have similar IR divergences. The IR divergences in the virtual correction will be canceled by the IR divergences from the counterterms and the real correction.

B. The real corrections to NLO

Note that here 'the NLO real correction'³ for the concerned process $e^- + e^+ \rightarrow B_c(B_c^*) + b + \bar{c}$ means to take into account the full contributions from the process $e^-(q_1) + e^+(q_2) \rightarrow B_c(B_c^*)(p_1) + b(p_2) + \bar{c}(p_3) + g(p_4)$ with

an additional gluon in final state but covering whole possible phase space.

Half of the Feynman diagrams for the real correction are shown in Fig.6 and the other half can be obtained from Fig.6 through interchanging the c -quark and b -quark lines. The correction to the relevant cross section can be written as:

$$d\sigma_{\text{Real}} = \frac{1}{4} \frac{1}{2s} \sum |M_{\text{Real}}|^2 d\Phi_4, \quad (5)$$

where M_{Real} is the sum of 24 terms relating to the 24 Feynman diagrams for the real correction. $|M_{\text{Real}}|^2$ can be formulated as

$$|M_{\text{Real}}|^2 = \sum_{i,j} M_{\text{Real},i}^* M_{\text{Real},j}, \quad (6)$$

where i, j vary from 1 to 24 corresponding to the 24 real correction Feynman diagrams.

There are IR divergences in the real correction, which are generated by the phase space integration, and they should be finally canceled by the IR divergences appearing in the virtual correction. It is easy to realize[14] that, the terms $M_{\text{Real},i}^* M_{\text{Real},j}$ are IR finite for the phase space integration unless $M_{\text{Real},i}$ and $M_{\text{Real},j}$ are the amplitudes corresponding to Feynman diagrams in which a real gluon is emitted from an external on-shell line, e.g., here the first 8 diagrams in Fig.6. At this step, let us divide the cross section of the real correction into two parts as

$$d\sigma_{\text{Real}} = d\sigma_{\text{Real}}^{\text{IR}} + d\sigma_{\text{Real}}^{\text{IR-finite}}, \quad (7)$$

where $d\sigma_{\text{Real}}^{\text{IR}}$ contains the terms in $\sum_{i,j} M_{\text{Real},i}^* M_{\text{Real},j}$ only when $M_{\text{Real},i}$ and $M_{\text{Real},j}$ are the amplitudes corresponding to Feynman diagrams in which a real gluon is emitted from an external on-shell line. Namely we can formulate $d\sigma_{\text{Real}}^{\text{IR}}$ as

$$d\sigma_{\text{Real}}^{\text{IR}} = \frac{1}{4} \frac{1}{2s} \sum |M_{\text{Real}}^{\text{IR}}|^2 d\Phi_4 \quad (8)$$

³ In literature, sometimes 'the NLO real correction' contains only the contributions from the process $e^+e^- \rightarrow B_c(B_c^*) + b + \bar{c} + g$ with the gluon g so soft or collinear to merge into b or \bar{c} jet.

where $M_{\text{Real}}^{\text{IR}}$ is the sum of the amplitudes corresponding to Feynman diagrams in which a real gluon is emitted from an external on-shell line. $d\sigma_{\text{Real}}^{\text{IR-finite}}$ contains the remaining terms in $\sum_{i,j} M_{\text{Real},i}^* M_{\text{Real},j}$, i.e., $(|M_{\text{Real}}^{\text{IR}}|^2 - |M_{\text{Real}}^{\text{IR}}|^2)$. Due to the fact that there is no divergence in $\sigma_{\text{Real}}^{\text{IR-finite}}$, we can calculate it in 4-dimensional space-time directly.

In order to extract the IR divergences in $\sigma_{\text{Real}}^{\text{IR}}$ precisely so as to cancel the IR divergences in virtual correction precisely, we adopt the two-cutoff phase space slicing method[15]. By this method, the integration on the phase space is divided into two sectors through introducing a very soft cut $\delta_s (\ll 1)$ on the energy of the emitting gluon (p_4^0). Then,

$$d\sigma_{\text{Real}}^{\text{IR}} = d\sigma_{\text{Real}}^{\text{IR,soft}} + d\sigma_{\text{Real}}^{\text{IR,hard}}, \quad (9)$$

where

$$d\sigma_{\text{Real}}^{\text{IR,hard}} = \frac{1}{4} \frac{1}{2s} \sum |M_{\text{Real}}^{\text{IR}}|^2 d\Phi_4|_{p_4^0 > \delta_s \sqrt{s}/2}, \quad (10)$$

and

$$d\sigma_{\text{Real}}^{\text{IR,soft}} = \frac{1}{4} \frac{1}{2s} \sum |M_{\text{Real}}^{\text{IR}}|^2 d\Phi_4|_{p_4^0 < \delta_s \sqrt{s}/2}. \quad (11)$$

To calculate $\sigma_{\text{Real}}^{\text{IR,soft}}$, the eikonal approximation is adopted to deal with the amplitudes involved in $M_{\text{Real}}^{\text{IR}}$, where the terms of $\mathcal{O}(\delta_s)$ in $\sigma_{\text{Real}}^{\text{IR,soft}}$ have been neglected [15, 16]. Under this approximation, the amplitude corresponding to the Feynman diagram where a real gluon emitted from an external line can be factorized as a Born factor multiplying an eikonal factor, and it is easy to check that the eikonal factors relating to the diagrams Real-5 and Real-6 of Fig.6 are canceled by the eikonal factors relating to the diagrams Real-7 and Real-8 of Fig.6 respectively at the leading order approximation in relative velocity $\mathcal{O}(v^0)$. Thus at last under the eikonal approximation we obtain

$$\sum |M_{\text{Real}}^{\text{IR}}|^2 = 4\pi\alpha_s C_F \mu^{2\epsilon} \left[\frac{-(p_2)^2}{(p_2 \cdot p_4)^2} + \frac{2p_2 \cdot p_3}{(p_2 \cdot p_4)(p_3 \cdot p_4)} - \frac{(p_3)^2}{(p_3 \cdot p_4)^2} \right] \sum |M_{\text{Born}}|^2. \quad (12)$$

Up-to corrections of $\mathcal{O}(\delta_s)$, the phase space for the soft sector can be factorized as [15]

$$d\Phi_4|_{p_4^0 < \delta_s \sqrt{s}/2} = d\Phi_3 \frac{d^{d-1}p_4}{2p_4^0 (2\pi)^{d-1}}|_{p_4^0 < \delta_s \sqrt{s}/2} \quad (13)$$

where $d\Phi_3$ denotes the element of the three-body phase space without emitting a gluon. Performing the integration over the momentum of the emitting gluon (p_4) in the soft sector, the differential cross section

$$d\sigma_{\text{Real}}^{\text{IR,soft}} = d\sigma_{\text{Born}} \frac{\alpha_s}{\pi} \Gamma(1 + \epsilon) \left(\frac{4\pi\mu^2}{s} \right)^\epsilon \left(\frac{A}{\epsilon} + B \right) \quad (14)$$

is obtained[17], where

$$\begin{aligned} A &= C_F \left[1 - \frac{\kappa (p_2 \cdot p_3)}{\kappa^2 m_b^2 - m_c^2} \ln \left(\frac{\kappa^2 m_b^2}{m_c^2} \right) \right], \\ B &= C_F \left\{ - \left[1 - \frac{\kappa (p_2 \cdot p_3)}{\kappa^2 m_b^2 - m_c^2} \ln \left(\frac{\kappa^2 m_b^2}{m_c^2} \right) \right] \ln(\delta_s^2) + \frac{1}{2\beta_b} \ln \left(\frac{1 + \beta_b}{1 - \beta_b} \right) + \frac{1}{2\beta_{\bar{c}}} \ln \left(\frac{1 + \beta_{\bar{c}}}{1 - \beta_{\bar{c}}} \right) \right. \\ &\quad \left. + \frac{2\kappa (p_2 \cdot p_3)}{\kappa^2 m_b^2 - m_c^2} \left[\frac{1}{4} \ln^2 \left(\frac{u^0 - |\mathbf{u}|}{u^0 + |\mathbf{u}|} \right) + \text{Li}_2 \left(1 - \frac{u^0 + |\mathbf{u}|}{v} \right) + \text{Li}_2 \left(1 - \frac{u^0 - |\mathbf{u}|}{v} \right) \right]_{u=p_3}^{u=\kappa p_2} \right\}, \quad (15) \end{aligned}$$

here

$$\begin{aligned} \beta_b &= \sqrt{1 - m_b^2/(p_2^0)^2}, \\ \beta_{\bar{c}} &= \sqrt{1 - m_c^2/(p_3^0)^2}, \quad (16) \end{aligned}$$

$$v = \frac{\kappa^2 m_b^2 - m_c^2}{2(\kappa p_2^0 - p_3^0)}, \quad (17)$$

and

$$\kappa = \frac{p_2 \cdot p_3 + \sqrt{(p_2 \cdot p_3)^2 - m_b^2 m_c^2}}{m_b^2}. \quad (18)$$

It can be checked precisely that the $1/\epsilon$ -terms in $d\sigma_{\text{Real}}^{\text{IR,soft}}$ defined by Eq.(14) are just canceled by those infrared $1/\epsilon$ -terms remained by the virtual correction Eq.(3).

μ	$\alpha_s(\mu)$	$\sigma_{\text{LO}}(\text{pb})$	$\sigma_{\text{NLO}}(\text{pb})$	$K \equiv \sigma_{\text{NLO}}/\sigma_{\text{LO}}$
$2m_b$	0.180	2.204	2.930	1.329
$m_Z/2$	0.132	1.185	2.059	1.738

TABLE II: The total cross section of $e^+e^- \rightarrow B_c^* + b + \bar{c} + X$ at the Z pole with two typical renormalization scales.

$\cos\theta$	-0.8	-0.6	-0.4	-0.2	0	0.2	0.4	0.6	0.8
$d\sigma/d\cos\theta(B_c, LO)$	1.066	0.892	0.759	0.667	0.617	0.608	0.639	0.711	0.825
$d\sigma/d\cos\theta(B_c, NLO)$	1.606	1.346	1.150	1.014	0.939	0.924	0.969	1.075	1.242
$K(B_c)$	1.506	1.509	1.515	1.520	1.522	1.520	1.516	1.512	1.505
$d\sigma/d\cos\theta(B_c^*, LO)$	1.507	1.254	1.060	0.926	0.853	0.839	0.884	0.990	1.156
$d\sigma/d\cos\theta(B_c^*, NLO)$	1.990	1.662	1.414	1.240	1.144	1.125	1.183	1.317	1.529
$K(B_c^*)$	1.320	1.325	1.334	1.339	1.341	1.341	1.338	1.330	1.323

TABLE III: The LO and NLO differential cross sections $\frac{d\sigma}{d\cos\theta}$ (in pb) of $e^-e^+ \rightarrow B_c(B_c^*) + b + \bar{c} + X$ and their ratio at various scattering angles ($\cos\theta$) at the Z pole ($\mu = 2m_b$).

Since there is no IR divergence in $d\sigma_{\text{Real}}^{\text{IR,hard}}$ due to the constraint $p_4^0 > \delta_s \sqrt{s}/2$, so we can calculate it in 4-dimensional space-time safely. Summing up $\sigma_{\text{Real}}^{\text{IR-finite}}$, $\sigma_{\text{Real}}^{\text{IR,soft}}$ and $\sigma_{\text{Real}}^{\text{IR,hard}}$, the requested σ_{Real} is obtained. Then with the Eqs.(2,3,7), the cross section σ_{NLO} of the process $e^+ + e^- \rightarrow B_c(B_c^*) + b + \bar{c} + X$, i.e. the production to QCD NLO accuracy, is achieved.

IV. NUMERICAL RESULTS

For numerical calculations, the necessary input parameters are taken as follows:

$$\begin{aligned}
m_b &= 4.9 \text{ GeV}, \quad m_c = 1.5 \text{ GeV}, \quad m_Z = 91.1876 \text{ GeV}, \\
\sin^2\theta_w &= 0.231, \quad \alpha = 1/128, \quad \Gamma_Z = 2.4952 \text{ GeV}, \\
|R_S(0)|^2 &= 1.642 \text{ GeV}^3,
\end{aligned} \tag{19}$$

$\alpha = \alpha(m_Z)$ is the electromagnetic coupling constant at $\mu = m_Z$; $R_S(0)$ is the radial wave function at the ori-

gin for $B_c(B_c^*)$, which can be taken from the potential model[1]. We apply the two-loop formula for the strong coupling constant $\alpha_s(\mu)$:

$$\alpha_s(\mu) = \frac{4\pi}{\beta_0 \ln(\mu^2/\Lambda_{QCD}^2)} \left[1 - \frac{\beta_1 \ln \ln(\mu^2/\Lambda_{QCD}^2)}{\beta_0^2 \ln(\mu^2/\Lambda_{QCD}^2)} \right], \tag{20}$$

where $\beta_1 = \frac{34}{3}C_A^2 - 4C_F T_F n_f - \frac{20}{3}C_A T_F n_f$ is the two-loop coefficient of the QCD β -function. According to $\alpha_s(m_Z) = 0.1185$ [18], we obtain $\Lambda_{QCD}^{n_f=5} = 0.233 \text{ GeV}$.

μ	$\alpha_s(\mu)$	$\sigma_{\text{LO}}(\text{pb})$	$\sigma_{\text{NLO}}(\text{pb})$	$K \equiv \sigma_{\text{NLO}}/\sigma_{\text{LO}}$
$2m_b$	0.180	1.576	2.387	1.515
$m_Z/2$	0.132	0.847	1.587	1.874

TABLE I: The total cross section of $e^+e^- \rightarrow B_c + b + \bar{c} + X$ at the Z pole with two typical renormalization scales.

Note that in the calculations here, we use FeynArts[19] for generating Feynman diagrams and amplitudes, FeynCalc[20] and FeynCalcFormLink[21] for carrying out the trace of color and Dirac matrices; while Apart[22] and FIRE[23] for conducting partial fraction and integration-by-parts (IBP) reduction. All the one-loop integrals are reduced into master integrals and the master integrals are computed in terms of LoopTools[24] numerically. The final phase-space integrations are computed with the help of the soft-ware Vegas[25].

The numerical results of the total cross sections at the colliding center-mass energy m_Z as well as the so-called K -factor (QCD) for the productions $e^+e^- \rightarrow B_c + b + \bar{c} + X$ and $e^+e^- \rightarrow B_c^* + b + \bar{c} + X$ with two different

renormalization scales, $\mu = 2m_b$ and $\mu = m_Z/2$, are put into the tables: TABLE I and TABLE II respectively, and the precise dependence of the cross sections on the renormalization scale μ for LO and NLO QCD is presented in Fig.7. It is shown in Fig.7 that the cross section of the production $e^+e^- \rightarrow B_c(B_c^*) + b + \bar{c} + X$ at the Z pole decreases by 46%(46%) at LO but by 34% (30%) at NLO when the renormalization scale μ changes from $2m_b$ to $m_Z/2$. Namely the dependence on renormalization scale μ is weakened a lot due to NLO correction. Whereas the dependence on the renormalization scale μ is still quite great for NLO, thus it seems that, to suppress the dependence on μ further, higher order corrections in QCD for the concerned production are requested.

z	0.183	0.269	0.355	0.441	0.527	0.613	0.699	0.785	0.871	0.957
$d\sigma/dz(B_c, LO)$	0.276	0.543	0.833	1.195	1.655	2.237	2.932	3.603	3.664	1.534
$d\sigma/dz(B_c, NLO)$	0.650	1.173	1.682	2.274	2.964	3.732	4.508	4.970	4.360	1.578
$K(B_c)$	2.355	2.160	2.019	1.903	1.791	1.668	1.538	1.379	1.190	1.029
$d\sigma/dz(B_c^*, LO)$	0.167	0.417	0.699	1.091	1.681	2.582	3.905	5.584	6.617	3.187
$d\sigma/dz(B_c^*, NLO)$	0.446	0.920	1.418	2.029	2.884	4.098	5.586	7.056	7.058	2.852
$K(B_c^*)$	2.671	2.206	2.029	1.860	1.716	1.587	1.430	1.264	1.067	0.895

TABLE IV: The LO and NLO differential cross sections $\frac{d\sigma}{dz}$ (in pb) of $e^-e^+ \rightarrow B_c(B_c^*) + b + \bar{c} + X$ and their ratios vs. various values of z (the energy fraction carried by $B_c(B_c^*)$) at the Z pole peak ($\mu = 2m_b$).

$(\sqrt{s} - m_z)(GeV)$	-5	-2.5	-1.5	-0.8	-0.4	-0.2	0	0.2	0.4	0.8	1.5	2.5	5
B_c (LO)	0.09	0.30	0.63	1.10	1.42	1.53	1.58	1.54	1.44	1.13	0.66	0.32	0.10
B_c (NLO)	0.13	0.46	0.95	1.66	2.13	2.32	2.39	2.33	2.18	1.71	1.00	0.49	0.15
B_c^* (LO)	0.12	0.42	0.88	1.54	1.98	2.14	2.20	2.16	2.02	1.59	0.92	0.46	0.14
B_c^* (NLO)	0.16	0.56	1.17	2.04	2.64	2.84	2.93	2.87	2.67	2.11	1.23	0.60	0.18

TABLE V: The total cross sections (in pb and with $\mu = 2m_b$) of $e^-e^+ \rightarrow B_c(B_c^*) + b + \bar{c} + X$ at the collision energies around m_z (Z -boson peak).

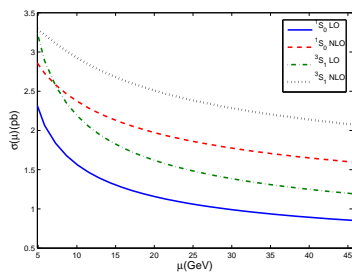


FIG. 7: The dependence of the total cross sections for $B_c(B_c^*)$ production on the renormalization scale μ at the Z pole to LO and NLO.

Moreover, we also with $\mu = 2m_b$ calculate the differential cross sections $d\sigma/d\cos\theta$, $d\sigma/dz$ and the relevant K -factor as well. Here θ is the angle between the momenta of the electron in initial state and the meson $B_c(B_c^*)$ in final state at center-of-mass system of the e^+, e^- collision and z is the ‘energy-fraction’ defined as $2k \cdot p_1/s$ (k is the momentum carried by Z boson).

The differential cross sections $d\sigma/d\cos\theta$ for the production of $B_c(B_c^*)$ meson with $\mu = 2m_b$ to LO and NLO, and the K factor as well are put in TABLE III. The differential cross section $d\sigma/d\cos\theta$ with renormalization scale $\mu = 2m_b$ is presented in Fig.8. It is shown by Fig.8 that due to the NLO QCD corrections the differential cross section $d\sigma/d\cos\theta$ changes only within a common factor K presented in TABLE III.

From Fig.8 the asymmetry in $d\sigma/d\cos\theta$ due to Z -boson mediation at the levels of LO and NLO can be seen very clear, which varies with the values of the electroweak mixing angle $\sin^2\theta_w$ for b and c quarks. When measuring the asymmetry and to suppress the experi-

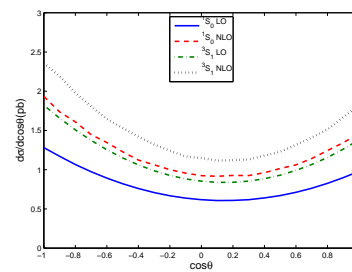


FIG. 8: The differential cross sections $\frac{d\sigma}{d\cos\theta}$ to LO and NLO for $e^-e^+ \rightarrow B_c(B_c^*) + b + \bar{c} + X$ at the Z pole ($\mu = 2m_b$).

mental systematic errors, similar to what done by LEP-I and SLC[26], one may introduce the forward-backward asymmetry A_{FB} for the B_c or B_c^* production as follows, although LEP-I and SLC is for measuring the forward-backward asymmetry for heavy quarks and leptons and here is for measuring the forward-backward asymmetry for the $B_c(B_c^*)$ production which relates to the electroweak mixing angle $\sin\theta_W$ for b and c quarks only:

$$A_{FB} = \frac{\sigma_F - \sigma_B}{\sigma_F + \sigma_B}, \quad (21)$$

where σ_F denotes the cross section for $\theta \in (0, \pi/2)$ and σ_B denotes the cross section for $\theta \in (\pi/2, \pi)$ thus we compute the forward-backward asymmetry A_{FB} for the production of B_c and B_c^* meson from LO to NLO:

$$\begin{aligned} A_{FB}^{LO}(B_c) &= -9.58 \times 10^{-2}, \\ A_{FB}^{NLO}(B_c) &= -9.50 \times 10^{-2}, \\ A_{FB}^{LO}(B_c^*) &= -9.97 \times 10^{-2}, \\ A_{FB}^{NLO}(B_c^*) &= -9.83 \times 10^{-2}. \end{aligned} \quad (22)$$

$(\sqrt{s} - m_Z)(\text{GeV})$	-5	-2.5	-1.5	-0.8	-0.4	-0.2	0	0.2	0.4	0.8	1.5	2.5	5
B_c	0.18	-0.35	-0.63	-0.53	0.06	0.33	0.79	1.24	1.64	2.11	2.21	1.91	1.39
B_c^*	0.19	-0.53	-0.92	-0.78	-0.12	0.41	1.04	1.67	2.22	2.88	3.01	2.60	1.88

TABLE VI: The contributions (in fb and with $\mu = 2m_b$) to the production due to the Feynman diagrams with a photon mediation to replace the Z -boson mediation at the collision energies around m_Z .

The forward-backward asymmetry A_{FB} for the production of B_c and B_c^* meson is about ten percent, that is easy to be seen experimentally.

The energy-fraction distributions of B_c and B_c^* production, $\frac{d\sigma}{dz}$, are also computed with $\mu = 2m_b$, and the precise values obtained for the distributions are put into TABLE IV and in Fig.9 for the relevant curves. One may see from TABLE IV that the K factors vary with the energy-fraction z quite a lot, and from Fig.9 that the maximum point of the z distributions is shifted to smaller z due to QCD NLO corrections.

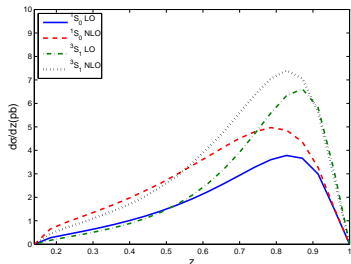


FIG. 9: The differential cross sections $\frac{d\sigma}{dz}$ to LO and NLO for $e^-e^+ \rightarrow B_c(B_c^*) + b + \bar{c} + X$ at the Z pole peak ($\mu = 2m_b$).

To be a reference and to see the variation of the total cross section at the collision energies around m_Z peak (within 5 GeV region), we also compute the cross section to LO and NLO with $\mu = 2m_b$, and put the result in TABLE.V.

By the way, we should note here that for the production of B_c and B_c^* by Z decay the relevant decay widths for $\Gamma_{Z \rightarrow B_c(B_c^*) + b + \bar{c} + X}$ can be easily ‘read out’ from the total cross sections of the production, $\sigma(e^+e^- \rightarrow B_c(B_c^*) + b + \bar{c} + X)$, at the Z pole peak with the contributions for photon mediation being ignored. In the literature there are the relevant decay widths, $\Gamma_{Z \rightarrow B_c(B_c^*) + b + \bar{c} + X}$, at LO and NLO[27, 28], thus we have made precise comparisons of the widths read out from the total cross sections with those computed directly from the Z decay in literature. In Appendix-A, the way how to ‘read out’ the decay widths $\Gamma_{Z \rightarrow B_c(B_c^*) + b + \bar{c} + X}$ respectively from the total cross sections $\sigma(e^+ + e^- \rightarrow B_c(B_c^*) + b + \bar{c} + X)$ at the Z pole is presented, and in Appendix-B careful comparisons are made. The situation is that the induced NLO decay width $\Gamma_{Z \rightarrow B_c + b + \bar{c} + X}$ is bigger than that in Ref.[27], but the induced NLO decay width $\Gamma_{Z \rightarrow B_c^* + b + \bar{c} + X}$ is consistent with that in Ref.[28].

In the above calculations the contributions from the

photon mediation are ignored. In order to see the ignored contributions the squared Feynman diagrams which have a photon mediation instead of a Z -boson mediation and the interference of the Feynman diagrams with a Z -boson mediation and those with a photon mediation should be computed. The two components: the amplitude with a photon mediation squared and the interference of those with a Z -boson mediation and with a photon mediation, and put the results in TABLE VI. From the results TABLE VI one may see that the contributions from the ones with a photon propagator (those squared and the interference) around the Z pole resonance are very small in comparison with the contributions from those with a Z -boson propagator, thus it may be conclude that the approximation ignoring the contributions from the Feynman diagrams with a virtual γ is quite good, furthermore since the precise values on the contributions estimated to QCD LO accuracy in TABLE VI are so small, so it is reasonable to believe that the conclusion will be still valid even the estimate on the contributions up-to QCD NLO accuracy.

V. DISCUSSIONS AND CONCLUSION

We have calculated the NLO QCD corrections to the production of B_c or B_c^* meson at e^+e^- colliders running near the Z pole. The results show that the NLO corrections are significant. The dependence on the renormalization scale μ for the cross sections at NLO level is suppressed in comparison with LO results. Precisely, the total cross section for the B_c (B_c^*) production at the Z -pole peak decreases about 46% (46%) for LO, and about 34% (30%) for NLO when μ changes from $2m_b$ to $m_Z/2$ accordingly. Namely, the dependence of the cross sections on the renormalization scale μ up-to NLO correction is still not small, so it means that to suppress the μ dependence further higher order QCD corrections are requested.

According to the present NLO QCD calculations, the conclusion obtained by LO calculations keeps valid. Namely to study the production $e^+e^- \rightarrow B_c(B_c^*) + b + \bar{c} + X$ experimentally in order to enhance the statistics of the relevant events the best energy region is around the Z pole peak for resonance enhancement and the collider still is requested to have so high luminosity i.e. higher than $10^{35} \text{ cm}^{-2}\text{s}^{-1}$, because up-to QCD NLO accuracy the cross sections for the production do not change much, i.e. still are of the order $\mathcal{O}(pb)$.

The computations and analyses here on the total cross

sections, the differential cross sections vs. angle, the forward-backward asymmetry and energy fraction distributions of the produced B_c and B_c^* mesons show that the shape of the angle distributions, the forward-backward asymmetry, the K -factor from the NLO QCD accuracy to the LO QCD accuracy change slightly, but the distribution on the energy fraction z changes sizable i.e. the maximum is shifted to smaller energy fraction (see TABLE. III, Figs. 8 and 9). Therefore, when experimentally the events have been collected numerously enough (it is accessible for a collider with so high luminosity as mentioned above), the characters in angle distributions and the forward-backward asymmetry etc for the production up-to NLO accuracy may be used not only to test of the theoretical predictions for the production but also as done by LEP-I and SLC to do the precision test of SM, e.g. to test the electro-weak mixing angle $\sin^2\theta_w$ etc.

Acknowledgments: We thank Jian-Xiong Wang and Rong Li for helpful discussions. This work was supported in part by Nature Science Foundation of China (NSFC) under Grant No. 11275243, No. 11275036, No. 11447601, No. 11535002 and No. 11675239

Appendix

A. The decay width $\Gamma(Z \rightarrow B_c(B_c^*) + b + \bar{c} + X)$ reduced from the total cross section $\sigma(e^+e^- \rightarrow B_c(B_c^*) + b + \bar{c} + X)$ at the energy of the Z -boson pole

The total cross section of the process $e^+e^- \rightarrow 'Z' \rightarrow B_c(B_c^*) + b + \bar{c} + X$ can be represented as

$$\sigma = \frac{1}{4} \frac{1}{2s} \frac{L^{\mu\nu} H_{\mu\nu}}{(s - m_Z^2)^2 + m_Z^2 \Gamma_Z^2}, \quad (23)$$

where Γ_Z is the total width of the boson Z , $L^{\mu\nu}$ is the leptonic tensor and

$$L^{\mu\nu} = a [q_1^\mu q_2^\nu + q_2^\mu q_1^\nu - (s/2)g^{\mu\nu}] + ibe^{\mu\nu\lambda\tau} q_{1\lambda} q_{2\tau}, \quad (24)$$

here

$$a = \frac{e^2(1 - 4\sin^2\theta_w + 8\sin^4\theta_w)}{2\sin^2\theta_w \cos^2\theta_w},$$

$$b = \frac{e^2(1 - 4\sin^2\theta_w)}{2\sin^2\theta_w \cos^2\theta_w}. \quad (25)$$

$H_{\mu\nu}$ is the hadronic tensor, which has been performed the phase space integration. $H_{\mu\nu}$ can only depend on k , and has following form

$$H_{\mu\nu} = H_1(s)g_{\mu\nu} + H_2(s)k_\mu k_\nu / s, \quad (26)$$

where $H_1(s)$ and $H_2(s)$ are scalar functions. Because there's no UV or IR divergence after considering the renormalization and the real correction, $H_1(s)$ and $H_2(s)$

are free of UV and IR divergences. Thus, all the derivations in the appendix are performed in 4-dimension. According to Eqs.(23), (24) and (26), we can obtain the cross section at the Z pole

$$\sigma = -\frac{aH_1(m_Z^2)}{8m_Z^2\Gamma_Z^2}, \quad (27)$$

here $\sqrt{s} = m_Z$.

The decay width of the process $Z \rightarrow B_c(B_c^*) + b + \bar{c} + X$ is

$$\Gamma = \frac{1}{3} \frac{1}{2m_Z} \Pi^{\mu\nu} H_{\mu\nu}, \quad (28)$$

where

$$\Pi^{\mu\nu} = -g^{\mu\nu} + k^\mu k^\nu / m_Z^2, \quad (29)$$

then we obtain

$$\Gamma = -\frac{H_1(m_Z^2)}{2m_Z}. \quad (30)$$

According to Eqs.(27) and (30), we obtain the relation

$$\Gamma = \frac{4m_Z\Gamma_Z^2}{a}\sigma. \quad (31)$$

Obviously from Eq.(31) one can obtain the decay width for $Z \rightarrow B_c(B_c^*) + b + \bar{c} + X$ from the total cross section of the relevant process $e^+e^- \rightarrow B_c(B_c^*) + b + \bar{c} + X$.

B. To compare the results for the decay $Z \rightarrow B_c(B_c^*) + b + \bar{c} + X$ up-to NLO

μ	$\Gamma_{\text{NLO}}(\text{Ours})$	$\Gamma_{\text{NLO}}(\text{Ref.}[27])$
$2m_b$	111.05 ± 0.09	78.45
$m_Z/2$	76.22 ± 0.04	62.53

TABLE VII: The derived width (in keV) for the decay $Z \rightarrow B_c + b + \bar{c} + X$ from the total cross section for the relevant production $e^+ + e^- \rightarrow B_c + b + \bar{c} + X$ with the same input parameters as those in Ref.[27]. The values in the last column of the table are copied from Ref.[27]. Here for the derived NLO width, the statistical errors from the numerical integration on the phase space are also presented.

There are calculations on the decay width for $Z \rightarrow B_c(B_c^*) + b + \bar{c} + X$ up-to NLO QCD in Refs.[27, 28], so here we do the comparisons on the decay width of theirs and those derived from our calculations for the total cross section of the production $e^+ + e^- \rightarrow B_c(B_c^*) + b + \bar{c} + X$ in terms of the way in Appendix-A.

The two-cutoff phase space slicing method for the phase space integration by introducing δ_s [12] is used as indicated by Eqs.(9,10,11) and δ_s is fixed as 10^{-6} finally according to the requirement for the method. So it would

μ	$\Gamma_{\text{NLO}}(\text{Ours})$	$\Gamma_{\text{NLO}}(\text{Ref.}[28])$
$2m_b$	118.48 ± 0.09	118.77
$m_z/2$	84.47 ± 0.05	84.60

TABLE VIII: The derived width (in keV) for the decay $Z \rightarrow B_c^* + b + \bar{c} + X$ from the total cross section for the relevant production $e^+ + e^- \rightarrow B_c^* + b + \bar{c} + X$ with the same input parameters as those in Ref.[28], and the values in the last column of the table are copied from Ref.[28]. Here for the derived NLO width, the statistical errors from numerical phase space integration are also presented.

be better that the errors generated by the calculation are presented precisely for the comparisons. Moreover, in or-

der to compare the results in Refs.[27, 28] with ours, we take the same parameters as those taken in Refs.[27, 28] and put the comparison results in TABLE VII and TABLE VIII.

From the tables, one may see that the results for NLO corrections of B_c production in [27] are different from ours, but those for NLO corrections of B_c^* production in [28] are consistent with ours.

-
- [1] E.J. Eichten and C. Quigg, Mesons with beauty and charm: Spectroscopy, Phys.Rev. D**49**, 5845 (1994) and references therein.
- [2] G.T. Bodwin, E. Braaten and G.P. Lepage, Rigorous QCD analysis of inclusive annihilation and production of heavy quarkonium, Phys. Rev. D **51**, 1125 (1995) [Erratum-ibid. D **55**, 5853 (1997)].
- [3] Chao-Hsi Chang and Yu-Qi Chen, Decays of the B_c Meson, Phys. Rev. D **49**, 3399 (1994); Chao-Hsi Chang, Yu-Qi Chen, Guo-Li Wang and Hong-Shi Zong, Decays of B_c Meson to a P -Wave Charmonium state χ_c or h_c , Phys. Rev. D **65**, 014017 (2002); A. Abd El-Hady, J. H. Muñoz and J. P. Vary, Semileptonic and non-leptonic B_c decays, Phys. Rev. D **62**, 014019 (2000); D. Ebert, R. N. Faustov and V. O. Galkin, Weak decays of the B_c meson to B_s and B mesons in the relativistic quark model, Eur. Phys. J. C **32**, 29 (2003); Phys. Rev. D **68**, 094020 (2003); Chao-Hsi Chang, Hui-Feng Fu, Guo-Li Wang, Jin-Mei Zhang, Some of semileptonic and nonleptonic decays of B_c meson in a Bethe-Salpeter relativistic quark model, Sci China-Phys Mech Astron **58**, 071001 (2015); Zhou Rui, Wen-Fei Wang, Guang-xin Wang, Lihua Song, Cai-Dian Lu, The $B_c \rightarrow \psi(2S)\pi, \eta_c(2S)\pi$ decays in the perturbative QCD approach, Eur. Phys. J. C **75**, 293 (2015).
- [4] N. Brambilla, et al. Heavy quarkonium: progress, puzzles, and opportunities, Eur. Phys. J. C **71**, 1534 (2011) and references therein.
- [5] N. Brambilla, et al. Heavy Quarkonium Physics, CERN-2005-005 20 June 2005, arXiv: hep-ph/0412158.
- [6] F. Abe, et al. (CDF Collaboration), Observation of the B_c Meson in $p\bar{p}$ Collisions at $\sqrt{s} = 1.8\text{TeV}$, Phys. Rev. Lett. **81**, 2432 (1998); Observation of B_c mesons in $p\bar{p}$ collisions at $\sqrt{s} = 1.8\text{TeV}$, Phys. Rev. D **58**, 112004 (1998).
- [7] C.-H Chang and Y.-Q Chen, The Production of B_c or \bar{B}_c associated with two heavy quark jets in Z^0 boson decay, Phys. Rev. D **46**, 3845 (1992); Erratum, Phys. Rev. D **50**, 6013 (1994); The B_c and \bar{B}_c mesons accessible to experiments by Z^0 boson decay, Phys. Letts. B **284**, 127-132 (1992).
- [8] P. Abreu, et al (DELPHI Collaboration), Search for the B_c meson, Phys. Letts. B **398**, 207 (1997); R. Barate, et al (ALEPH Collaboration), Search for the B_c meson in hadronic Z^0 decay, Phys. Letts. B **402**, 213 (1997); K. Ackerstaff, et al (OPAL Collaboration), Search for the B_c meson in hadronic Z^0 decay, Phys. Letts. B **420**, 157 (1998).
- [9] X.-C. Zheng, C.-H. Chang and Z. Pan, Production of doubly heavy-flavored hadrons at e^+e^- colliders, Phys. Rev. D **93**, 034019 (2016).
- [10] M. Beneke and V.A. Smirnov, Asymptotic expansion of Feynman integrals near threshold, Nucl. Phys. B**522**, 321 (1998).
- [11] J.G. Korner, D. Kreimer and K. Schilcher, A Practicable γ_5 -scheme in dimensional regularization, Z. Phys. C**54**, 503 (1992).
- [12] T. Kinoshita, Mass Singularities of Feynman Amplitudes, J. Math. Phys. **3**, 650 (1962).
- [13] S. Dittmaier, Separation of soft and collinear singularities from one-loop N-point integrals, Nucl. Phys. B**675**, 447 (2003).
- [14] G. Grammer, Jr. and D. R. Yennie, Improved Treatment for the Infrared-Divergence Problem in Quantum Electrodynamics, Phys. Rev. D **8**, 4332 (1973).
- [15] B.W. Harris and J.F. Owens, Two cutoff phase space slicing method, Phys. Rev. D **65**, 094032 (2002).
- [16] A. Bassetto, M. Ciafaloni, and G. Marchesini, Jet Structure and Infrared Sensitive Quantities in Perturbative QCD, Phys. Rept. **100**, 201 (1983).
- [17] A. Denner, Techniques for the Calculation of Electroweak Radiative Corrections at the One-loop Level and Results for W-physics at LEP-200, Fortschr. Phys. **41**, 307 (1993).
- [18] K.A. Olive, et al. (Particle Data Group), Review of particle physics, Chin.Phys. C**38**, 090001 (2014).
- [19] T. Hahn, Generating Feynman diagrams and amplitudes with FeynArts 3, Comput. Phys. Commun **140**, 418 (2001).
- [20] R. Mertig, M. Bohm and A. Denner, Feyn Calc - Computer-algebraic calculation of Feynman amplitudes, Comput. Phys. Commun **64**, 345 (1991).
- [21] F. Feng and R. Mertig, FormLink/FeynCalcFormLink: Embedding FORM in Mathematica and FeynCalc, arXiv:1212.3522.
- [22] F. Feng, \$Apart: A Generalized Mathematica Apart

- Function, *Comput. Phys. Commun* **183**, 2158 (2012).
- [23] A.V. Smirnov, Algorithm FIRE - Feynman Integral Reduction, *J. High Energy Phys.* **10**, 107 (2008).
- [24] T. Hahn and M. Perez-Victoria, Automatized one loop calculations in four-dimensions and D-dimensions, *Comput. Phys. Commun* **118**, 153 (1999).
- [25] G.P. Lepage, A New Algorithm for Adaptive Multidimensional Integration, *J. Comp. Phys.* **27**, 192 (1978).
- [26] C. Patrignani et al (Particle Data Group), *Chin. Phys. C.* **40**, 100001(2016).
- [27] C.-F. Qiao, L.-P. Sun, R.-L. Zhu, The NLO QCD Corrections to B_c Meson Production in Z^0 Decays, *JHEP* **08**, 131 (2011).
- [28] J. Jiang, L.-B. Chen, C.-F. Qiao, QCD NLO corrections to inclusive B_c^* production in Z^0 decays, *Phys. Rev. D* **91**, 034033 (2015).